

Simultaneous HST/ASCA Observations of LMC X-4: X-ray Ionization Effects on a Stellar Wind

S. D. Vrtilek¹, B. Boroson

Center for Astrophysics, 60 Garden St., Cambridge, MA. svrtilek@cfa.harvard.edu,
bboroson@cfa.harvard.edu

F. H. Cheng²

Department of Astronomy and Astrophysics, Villanova University, Villanova, PA 19085.
fcheng@ucis.vill.edu

R. McCray

JILA, Campus Box 440, University of Colorado, Boulder, CO 80309.
dick@jila.colorado.edu

and

F. Nagase

ISAS, 3-1-1, Yoshinodai, Sagamihara, Kanagawa 229, Japan. nagase@astro.isas.ac.jp

ABSTRACT

We present first results from simultaneous ultraviolet (HST/GHRS) and X-ray (ASCA) observations of the 13.5s pulsar LMC X-4 taken in 1996 May. The ASCA observations covered 1.12 binary orbits (1.58 days) and the HST observations were centered on this for roughly 0.4 orbital phase coverage (0.56 days). The GHRS data are the highest resolution (both temporal and spectral) ultraviolet spectra ever taken of LMC X-4. With generally-accepted parameters

¹Visiting Professor, Department of Astronomy, University of Maryland, College Park, MD 20742

²Center for Space Science, Shanghai Jiao Tong University, Shanghai, 200023, People's Republic of China

for the source, fits to the UV continuum using a model that incorporates X-ray heating of the companion star and the accretion disk yields a mass accretion rate $\dot{M} = 4.0 \times 10^{-8} M_{\odot} \text{ yr}^{-1}$; the X-ray luminosity implied by this value is consistent with the X-ray flux measured during simultaneous observations ($3.2 \times 10^{-10} \text{ ergs cm}^{-2} \text{ s}^{-1}$). The model accurately predicts observed B magnitude and ultraviolet variations over both orbital and long-term periods. The ultraviolet P-Cygni lines show dramatic changes with orbital phase with strong broad absorption near X-ray eclipse and narrow absorption when the X-ray source is in the line-of-sight. We interpret this as a result of X-ray photoionization of the stellar wind; when the neutron star is in front of the normal star, the wind absorption disappears and mainly the photospheric absorption lines are visible. The X-ray pulse period measured during our observations, $13.5090 \pm 0.0002 \text{ s}$, is consistent with steady spin-down over the past 10 years. No pulsations were detected in the ultraviolet observations with upper limits to the pulsed fraction around NV and CIV of 1.8% and 2.7% in the continuum and 12.4% and 7% in the absorption troughs.

Subject headings: accretion, accretion disks— binaries: eclipsing— pulsars: individual (LMC X-4)— sars: neutron and mass-loss

1. Introduction

LMC X-4 is a 13.5s pulsar orbiting a $20 M_{\odot}$ O7 III-V companion every 1.4 days (Kelley *et al.* 1983; Ilovaisky *et al.* 1984). The system exhibits a long term cycle with a roughly 30-day period (Lang *et al.* 1981; Ilovaisky *et al.* 1984) similar to the 35-day period of Her X-1. Although the high-mass companion of LMC X-4 implies the presence of a wind, LMC X-4 has many properties in common with the disk-fed system Her X-1. In both systems the long term periods are roughly 20 times the orbital periods. Both systems

are fully eclipsing (Tananbaum *et al.* 1972; Li *et al.* 1978); show a power-law spectrum with a soft X-ray “excess” in the 0.5-10 keV band (Dennerl 1989); optical light curves with a power spectrum that shows power at the sum of the orbital and long term frequencies, but not in the difference, implying that the long-term variations are due to precession of an accretion disk (Ilovaisky *et al.* 1984); and correlation between times of low hard X-ray luminosity and episodes of spindown (Dennerl 1991; Wilson *et al.* 1994). The optical lightcurves of LMC X-4 show changes in peak-to-peak amplitude of up to 40% relative to the mean over the 30-day period whereas the optical lightcurves of Her X-1 show less than 20% change in peak-to-peak amplitude over the 35-day cycle. For LMC X-4 the X-ray flux varies by a factor of 60 between the high and low states of the 30-day period; however, the flux of scattered X-rays, measured during X-ray eclipses, remains unchanged throughout the 30 day cycle (Woo *et al.* 1995), implying that the low state is not caused by a decrease in X-ray luminosity but by attenuation in intervening matter. LMC X-4 also displays flares which typically occur once a day (Dennerl 1989; Levine *et al.* 1991; Woo *et al.* 1996). The X-ray luminosity during the flares rises to ~ 5 times the Eddington luminosity and the spectrum changes from a power law to a very hot thermal spectrum.

There are several mechanisms that could cause the UV continuum or lines to vary with the 13.5 second neutron star rotation period. In Vela X-1 it has been shown that the Si IV and NV P Cygni lines of Vela X-1 vary with the 283 second pulsar period, presumably as a result of time-dependent photoionization of the stellar wind by the X-rays (Boroson *et al.* 1996a). The UV continuum could pulsate as a result of X-ray heating of either the normal star or the accretion disk, as is the case in Her X-1 (Boroson *et al.* 1996b).

Here we present coordinated ultraviolet and X-ray observations of LMC X-4 taken with the GHRS on HST and with the GIS and SIS on ASCA. The high temporal resolution of the GHRS allowed us to search for a manifestation of the pulsations in the UV and the high spectral resolution allows us to study the geometry of the system as reflected in the line profiles. Some results from an ASCA observation covering a full binary orbit

taken an year earlier are also presented. We compare the HST data as well as archival IUE data with models predicting UV continuum emission from the X-ray heated disk and star that has been successfully applied to the Her X-1 system. We interpret the dramatic changes with orbital phase observed in the ultraviolet spectra in terms of the effects of X-ray photonization on the stellar wind of the normal companion. The observations and analysis are described in section 2 and our interpretation is discussed in section 3.

2. Observations and Analysis

Figure 1 shows the location of our observation in comparison with the one-day averaged lightcurves obtained from the All Sky Monitor on XTE and the same data folded with the long term ephemeris and period of Dennerl *et al.* (1992). This indicates that our simultaneous HST and ASCA observations occurred during the high state of the 30-day cycle, corresponding to a phase coverage of $\phi_{30\text{-day}}=0.20\text{-}0.22$.

The ASCA lightcurves and HST coverage are plotted on Figure 2. HST took eight separate observations, but as the target was nearly in HST’s Continuous Viewing Zone the gaps between the observations are small. A journal of the observations is given in Table 1. HST captured an eclipse egress that did not have simultaneous X-ray coverage. The HST observations were taken with the GHRS G160M grating centered alternately at 1240 Å (N V) and 1550 Å (C IV) in the RAPID mode with a time resolution of 0.5s. Our use of the GHRS RAPID mode prevented us from over-sampling the spectrum, checking for bad counts, and correcting for the Doppler shift due to the spacecraft orbit. The observed flux in the NV $\lambda 1240$ line measured with IUE (van der Klis *et al.* 1982) ranges from $F \approx 1 \times 10^{-12} \text{ergs cm}^{-2} \text{s}^{-1}$ at minimum ($\phi_{orb} \approx 0.5$) to $F \approx 3 \times 10^{-12} \text{ergs cm}^{-2} \text{s}^{-1}$ at maximum ($\phi_{orb} \approx 0.9$). The fluxes measured from our observations are listed in Table 1.

The 1996 ASCA observations caught an eclipse ingress and two pre-eclipse dips that did not have simultaneous UV coverage. The 1994 ASCA observations covered more than a full binary orbit including an eclipse. Detailed studies of the ASCA observations will

appear elsewhere (Boroson *et al.* 1997b). No flares occurred during either the 1994 or 1996 ASCA observations although each covered more than a binary orbit and flares are reported to occur roughly once a day. It is possible that flares (which last roughly 30 minutes) occurred during the data gaps (roughly 40-50 minutes) due to earth occultation.

2.1. Continuum Fits

A model involving X-ray heating of the disk and star as previously applied to Her X-1 (Cheng, Vrtilik, & Raymond 1995) was adapted for use with LMC X-4. Changes to the model from that described in Cheng, Vrtilik, & Raymond are inclusion of both gravity darkening and limb darkening effects (important for the massive companion in LMC X-4) as well as a different reddening curve towards the LMC (Nandy *et al.* 1981). We use a distance to the source of 50 kpc and an E_{B-V} of 0.05. The companion star is modelled as a $20 M_{\odot}$ O7III star with an effective temperature of 35,000K and IUE spectra of stars of varying temperature are used to determine the spectral shape at different points on the star and disk surface. Predictions of the model from the ultraviolet and optical B band are shown in Figure 3. We are using archival IUE data for comparison, hence we restrict ourselves to the region near C IV since the presence of strong geocoronal Lyman Alpha prevents accurate determination of the IUE flux near N V. In addition our model, which is constructed to predict continuum emission, consistently overpredicts the flux near N V in this system; this is likely due to the presence of a stellar wind—not included in the model—which results in strong absorption at N V. Because the 30.25d period has a large uncertainty the long term phase of the IUE observations cannot be determined. The ultraviolet data including the current observations and all archival IUE observations fall within extremes given by a lower limit to \dot{M} of $3.2 \times 10^{-9} M_{\odot} \text{ yr}^{-1}$ and an upper limit of $1.0 \times 10^{-7} M_{\odot} \text{ yr}^{-1}$. The best fit curve to the HST continuum data (shown as filled triangles) corresponds to an \dot{M} of $4.0 \times 10^{-8} M_{\odot} \text{ yr}^{-1}$. There is uncertainty in the flux level, both for the model and the data. Our HST continuum determination is based on a

very narrow wavelength band since the observations were centered on lines and the total available bandpass was only 37\AA for the spectral resolution we required; the HST data are absolute flux calibrated to only 10%; there is a difference in resolution between IUE and GHRS. As for the model, the uncertainties in the reddening and stellar temperature can shift the flux. The fluxes near C IV and N V show a similar flux vs. orbit trend. The relative errors in flux are likely to be much smaller than the overall flux normalization.

The change in peak-to-peak amplitude of the optical flux from the 30-day low to the 30 day high predicted by the model is consistent with that observed (Ilovaisky *et al.* 1984). Figure 3b shows the extremes over the 30.25 day cycle for B magnitude variations and Figure 3c shows the model predictions at the X-ray on and off states for a given \dot{M} reproducing the variations shown by Ilovaisky *et al.* 1984 in their Figure 1. During binary eclipse the total UV and optical flux is due to the companion star. During the time of maximum UV flux (binary phase 0.75) for the highest \dot{M} the contribution from the disk is 8% and from the heated star 10%. A comprehensive presentation of the fits to individual IUE spectra and archival optical data will appear in a later paper (Preciado *et al.* 1997).

The X-ray spectra obtained by ASCA are consistent with a power law of photon index $\alpha = 0.63 \pm 0.02$, a 0.180 ± 0.006 keV blackbody, and an iron line at 6.54 ± 0.03 keV with an equivalent width of 99 ± 25 eV, typical for this source over the energy range observed. The 2-10 keV flux is $2.9 \times 10^{-10} \text{ ergs s}^{-1} \text{ cm}^{-2}$ with about 10% changes from the mean during the period of observations. The luminosity obtained from the \dot{M} measured with the UV continuum fits, using $L_x = 0.5GM\dot{M}/r$, is consistent with the luminosity implied by this flux.

2.2. Spectral Features

Figure 4 shows the N V and C IV line profiles at four orbital phases each; these are different for the two lines since they could not be observed simultaneously at this spectral resolution. These two lines are the strongest in the UV spectrum and are known from IUE

observations to be strongly and weakly phase dependent, respectively. The C IV profiles show little evolution from binary phase 0.15-0.49. At binary phase 0.11, the observation closest to the X-ray eclipse (binary phase 0.0), we see broad absorption in the N V doublets. The maximum velocity at this phase (1150 km/s) is reasonable for a terminal velocity for the wind however it is likely that by phase 0.11 some ionization has already taken place and terminal velocities of up to 1300 km/s are possible (Borson *et al.* 1997a). As we progress in phase towards seeing more of the X-ray source we find that the broad absorption disappears and what remains are relatively narrow absorption profiles. The width of the residual absorption left at phase 0.41 in N V is consistent with the width of the optical lines which Hutchings *et al.* attributed to the photosphere. Comparison with low-resolution IUE archival data suggests that the variations are phase dependent effects, presumably arising in the geometry-dependent interaction between the X-ray source and stellar wind.

Interstellar absorption lines from S II $\lambda\lambda$ 1250.578, 1253.805 are visible in our exposures in the wavelength region near N V $\lambda\lambda$ 1238, 1242. The velocities of these absorption lines (heliocentric redshifts are consistent with zero within the errors of our measurement) suggest that they arise in gas within the Galaxy, and not in the LMC (where we would expect velocities of the order 280-320 km s⁻¹; Bomans *et al.* 1996). The narrow C IV absorption lines are superimposed on broader absorption features, which we interpret as arising in the photosphere of the O star in the LMC X-4 system. As a result of the overlap, the velocity and especially the equivalent widths of the interstellar C IV lines are uncertain. The heliocentric redshifts of the C IV lines are also consistent with zero within the uncertainties of our measurement implying that the C IV absorber is also within the Galaxy.

There is no evidence for a C IV absorber associated with LMC X-4, which might be expected if the X-ray source photoionizes surrounding interstellar gas (McCray, Wright, and Hatchett 1977). The N V line at $\phi = 0.41$ shows what appears to be a narrow feature at the base of the absorption due to the blue doublet component. However, observations

at higher signal-to-noise ratio are needed to establish that this results from an interstellar feature and not merely a fluctuation in the photospheric line profile.

2.3. Search for Pulsations

The pulse periods that we measured from ASCA data of 1994 (13.5069 ± 0.0002 s) and 1996 (13.5090 ± 0.0002 s) are consistent with spin-down over the past 10 years (Figure 5). While earlier observations are scant they indicate that sometime between 10 and 20 years ago LMC X-4 went through a period of spin-up. Such rapid, erratic, changes from spin-up to spin-down are expected from equilibrium rotators (Chakrabarty *et al.* 1997), systems in which the spin period equals the Kepler period near the inner boundary of the accretion disk.

We searched for pulsations in the UV spectrum at the 13.5 second pulsar period using an analysis of variance (ANOVA) method (Davies 1990, 1991). This approach, which involves binning the data over trial periods, is well-suited to data with gaps or with non-uniform readout times. To detect pulsations from the accretion disk, we need to subtract the changes in light-travel time from the orbiting pulsar to the orbiting HST from the uniform readout times of the GHRS. Thus we report only the ANOVA method and not a power-spectral search to find pulsations from material moving with the neutron star.

From the 4 HST orbits we find a 5σ limit of 1.8% for the fractional peak-to-peak pulse amplitude in the continuum centered at 1240\AA surrounding the NV line. For the continuum surrounding CIV, the limit is 2.7%. Our limits for pulsation in the P Cygni absorption troughs are 12.4% in the NV line and 7% in the CIV line.

3. Discussion and Conclusions

A model that incorporates X-ray heating of the companion star and the accretion disk provides good fits to the continuum UV emission from LMC X-4. The value of \dot{M} derived from GHRs observations is consistent with that from X-ray flux measured during simultaneous observations. Owing to the size and temperature of the companion the major contribution to the ultraviolet and optical flux is the unheated companion star. At maximum light (binary phases 0.25 and 0.75) the contribution of the unheated star is 82%; heating of the primary contributes 10% and the disk 8%.

Although we captured no flares during our observations the X-ray heating model can accommodate flares by using unsteady accretion from the stellar wind. During flares the intensity can increase by factors of up to 20 for times ranging from ~ 20 s to 45 minutes, resulting in super Eddington luminosities (Dennerl 1989; Woo *et al.* 1995). The necessary \dot{M} is $3.2 \times 10^{-7} M_{\odot} \text{ yr}^{-1}$ and implies a range of a factor of 100 in \dot{M} for LMC X-4. By contrast the flaring states of Z-source LMXBs such as Sco X-1 and Cyg X-2, where the flaring state is also associated with super-Eddington accretion, are produced with changes of only a factor of 2-4 in \dot{M} ; this is because Sco X-1 and Cyg X-2 are disk fed systems normally accreting at just under the Eddington limit.

It is possible that the greater range and overall greater \dot{M} required for LMC X-4 is due to some intrinsic difference between X-ray binaries in the Magellanic Clouds compared with systems within our own Galaxy. The mean luminosity of those sources in the Clouds which have massive OB-type companions similar to LMC X-4 is 50 times that of the counterparts in our Galaxy (van Paradijs & McClintock 1995). It has been suggested that this is due to the lower abundances of metals in the Clouds. One linking mechanism is the effect of X-ray heating of gas as it falls toward a compact object: this depends strongly on the atomic number Z via the photoelectric cross section ($\sigma \propto Z^4$). For spherical accretion, such heating can seriously impede the accretion flow and thereby reduce the limiting luminosity to a value far below the Eddington limit; so the LMC sources may be

more luminous because their low- Z accretion flow is less impeded by heating. A second metallicity dependent effect takes place in wind-fed systems. The accretion rate depends sensitively on the velocity of the stellar wind; all available evidence indicates that the terminal wind velocity decreases with Z . Such behavior is predicted by successful theories of radiation-driven stellar winds (Kudritzki & Hummer 1990; Kudritzki *et al.* 1991). In this case the lower metallicity in the LMC means a lower terminal velocity, a higher \dot{M} and a more luminous X-ray source.

The dramatic orbital variations shown by the N V profiles can be interpreted in terms of X-ray photoionization of the stellar wind from the companion. The narrow absorption lines shown in Figure 4d can be attributed to the surface of the companion star and the broad lines to the wind. In this scenario, the X-ray source ionizes nearly the entire stellar wind that is not in the shadow of the companion star, so that when the neutron star is in front of the normal star, the wind absorption disappears and mainly the photospheric absorption lines are visible. It is only near phase 0.0, i.e. during X-ray eclipse, that the broad lines that reveal the high wind velocities become visible. Detailed fits to the line profiles with a model that takes into account the structure of the wind and its influence on spectral features will be presented in a later paper (Boroson *et al.* 1997a).

The pulse amplitude in the X-rays is lower in LMC X-4 (the pulsed fraction of LMC X-4 is 10% in quiescence) than in Her X-1 and Vela X-1. In Her X-1 the X-ray pulsed fraction is close to 50% and UV continuum pulsations have an amplitude of $\sim 0.5\%$ (Boroson *et al.* 1996). If LMC X-4 resembles Her X-1 than we would expect UV continuum pulsations with an amplitude of $\sim 0.1\%$, which is below our detection limit. The narrow wavelength regions surrounding the lines provided too low a count rate to detect pulsations similar to those seen in other systems. In Vela X-1 the pulsed fraction for 2-10 keV X-ray is 0.3, and, while no continuum pulsations were detected in the UV using FOS observations, 3% pulsations in the P-Cygni lines were detected. P Cygni line pulsations, seen in Vela X-1, may be smeared by light travel time in LMC X-4, owing to a more extended X-ray photoionized region.

The STIS, recently installed on HST, extends in several significant ways the ultraviolet capabilities that became available with the GHRS: with the echelle grating it is possible to sample continuously a broad region (600\AA) of the spectrum at greater spectral resolution than with the GHRS. Observations with the STIS that cover binary phase 0.0 can confirm our interpretation of the line profiles, provide improved measures of the continuum, and enable a more sensitive search for UV manifestation of the X-ray pulses.

Until recently, long-term approximately-periodic variability attributed to disk precession has been known for only three systems: Her X-1, LMC X-4, and SS433. XTE observations suggest similar long-term behavior in SMC X-1 and Cyg X-2 (Levine *et al.* 1996; Wijnands, Kuulkers, & Smale 1996). The interpretation of these periods in terms of disk precession has been questioned by several authors including, e.g., Kondo *et al.* 1983, who showed that precession of a disk controlled by the gravitational fields of the neutron and companion stars is untenable: any induced precession disappears rapidly because of differential precession within the disk. Recently Iping and Petterson (1990) proposed that the behavior attributed to precession is maintained by the influence of the X-ray emission on the structure of the disk. Accordingly, in these systems, the tendency of disks to undergo periodic changes in their orbital orientations is more appropriately termed radiation-driven warping. Iping and Petterson’s primary result, that strong central illumination can maintain disk warping, has been obtained analytically by Pringle (1996) and Maloney, Begelman, & Pringle (1996). The success of our X-ray heated star plus warped disk model in fitting the optical, UV, and X-ray lightcurves for both the orbital and long-term periods of Her X-1 and LMC X-4 supports an interpretation in terms of radiation-driven warping.

Based on observations with the NASA/ESA *Hubble Space Telescope*, obtained at the Space Telescope Science Institute, which is operated by the Association of Universities for Research in Astronomy, Inc., under NASA contract GO-05874.01-94A. We are grateful for quick-look results provided by the ASM/RXTE team. SDV and BB were supported in

part by NASA (NAG5-2532, NAGW-2685), and NSF (DGE-9350074).

References

- Bomans, D.J., DeBoer, K.S., Koornneef, J., & Grebel, E.K. . 1996, *A&A* 313, 101
- Boroson, B., McCray, R., Kallman, T.R., & Nagase, F. 1994, *ApJ*, 465, 940.
- Boroson, B., McCray, R., Kallman, T., & Nagase, F. 1996a, *ApJ*, 465, 940.
- Boroson, B., Vrtilik, S.D., McCray, R., Kallman, T., & Nagase, F. 1996b, *ApJ*, 473 1079.
- Boroson, B., Vrtilik, S.D., Kallman, T., & McCray, R. 1997a, in preparation.
- Boroson, B., Vrtilik, S.D., Xu, C., Kelley, R., & Stahle, C. 1997b, in preparation.
- Chakrabarty, D. *et al.* 1997, *ApJ*, 474, 414.
- Cheng, F.H., Vrtilik, S.D., & Raymond, J.C. 1995, *ApJ*, 452, 825.
- Davies, S.R. 1990, *MNRAS*, 244, 93.
- Davies, S.R. 1991, *MNRAS*, 251, 64p.
- Dennerl, K. 1989, PhD thesis at Max Planck Institute for...(D89).
- Dennerl, K. 1989, in 23rd ESLAB Symp., ed. J. Hunt & B. Battrock (Noordwijk:ESA-ESTEC), 39.
- Dennerl, K. *et al.* 1992, in *Lecture Notes in Physics*, 416, *New Aspects of Magellanic Cloud Research*, ed. B. Baschek, G. Klare, & J. Lequeux (Berlin: Springer), 74.
- Heemskerk, M.H.M., & van Paradijs, J. 1989, *A&A*, 223, 154.
- Ilovaisky, S.A., Chevalier, C., Motch, C., Pakull, M., Van Paradijs, J., & Lub, J. 1984, *A&A*, 140, 251.
- Iping, R.C., & Petterson, J.A. 1990, *A&A*, 239, 221.
- Kelley, R.L., Jernigan, J.G., Levine, A., Petro, L.D., & Rappaport, S. 1983, *ApJ*, 264, 568.
- Kondo, Y., Van Flandern, T.C., & Wolff, C.L. 1983, *ApJ*, 273, 716.
- Lang, F. L., *et al.* 1981, *ApJ*, 246, L21.
- Levine, A. M., Bradt, H., Cui, W., Jernigan, J. G., Morgan, E. H., Remillard, R., Shirey, R. E., & Smith, D. A. 1996, *ApJ*, 469, L33.
- Levine, A., Rappaport, S., Putney, A., Corbet, R., & Nagase, F. 1991, *ApJ*, 381, 101.
- Li, F. *et al.* 1978, *Nature*, 271, 38.
- Maloney, P. R., Begelman, M. C., & Pringle, J. E. 1996, *ApJ*, 472, 582.
- McCray, R., Wright, C., and Hatchett, S. 1977, *ApJ*, 211, L29.

- Nandy, K, Morgan, D.H., Willis, A.J., Wilson, R., & Gondhalekar, P.M. 1981, MNRAS, 196, 955.
- Preciado, M., Boroson, B., Vrtilik, S.D., & Raymond, J.C. 1997, in preparation.
- Pringle, J.E. 1996, MNRAS, 281, 357.
- Tananbaum, H., et al. 1972, ApJ 174, L143.
- van der Klis, M. *et al.* 1982, A&A, 106, 339.
- van Paradijs, J. & McClintock, J.E., 1995, in X-ray Binaries, eds. W.H.G. Lewin, J. van Paradijs, & E.P.J. van den Heuvel, Cambridge University Press: Cambridge.
- Wijnands, R. A. D., Kuulkers, E., & Smale, A. P. 1996, ApJ, 473, L45.
- Wilson, R.B., Finger, M.H., Pendleton, G.N., Brigg, M., & Bildsten, L. 1994, in The Evolution of X-ray Binaries, eds. S.S. Holt, & C. S. Day, AIP Press: New York.
- Woo, J.W., Clark, G.W., & Levine, A.M. 1995, ApJ, 449, 880.
- Woo, J.W., Clark, G.W., Levine, A.M., Corbet, R.H., & Nagase, F. 1996 ApJ 467, 811

Figure Captions

Figure 1. (a) One day averages of the flux observed from LMC X-4 with the All Sky Monitor on board the ROSSI X-ray Timing Explorer. (Quick-look results were provided by the ASM/RXTE team.) The arrow indicates the time of the simultaneous HST/ASCA observations, and the horizontal bar represents one 30.25 day interval. (b) The data from (a) (light lines) with the lightcurve from (c) (dark lines) superposed. (c) The data from (a) folded with the ephemeris for the long-term period provided by Dennerl *et al.* 1992 ($P_{30} = 30.25 \pm 0.03$ d and $\phi_{30}^0 = \text{JD } 2,448,226.0$). Arrow indicates the phase of the simultaneous HST/ASCA observations. The errors are 1σ from counting statistics.

Figure 2. (a) The exposure times of the HST observations which covered the binary phases 0.08-0.49 (start time = JD 2,450,228.44). The first observation is N V and is alternated with C IV. (b) ASCA lightcurves (0.5-10 keV): observations covered the binary phases 0.75-1.84 (start time = JD 2,450,227.92) determined from the ephemeris of Woo *et al.* (1996) with $P_{orb} = 1.40840249 \pm 6.0 \times 10^{-7}$ d and $\phi_{orb}^0 = \text{JD } 2,446,729.84878 \pm 0.0041$ d.

Figure 3. (a) Average UV continuum flux near C IV *vs.* binary phase. The solid squares represent the GHRS observations. The open triangles are archival IUE data. The dashed line represents a 30.25 day phase when the X-ray flux is in the low state; the solid line a 30.25d phase during an X-ray high state; and the dotted line represents the best fit continuum for the GHRS observations. (b) The B magnitude predictions of the model for the three states depicted in 3a. (c) The B magnitude predictions for a given \dot{M} during the X-ray on and off states. (b) and (c) should be compared with Figure 1 in Illovaisky *et al.* 1984.

Figure 4. The GHRS observations of N V and C IV.

Figure 5. The pulse period history of LMC X-4.

Table 1: Log of GHRS Observations

HST		Orbital		Wavelength	Continuum
Observation	Start time	phase ¹	Duration	range	Flux
Number	(JD-2,450,000)	at midpoint	(s)	(Å)	(ergs cm ⁻² s ⁻¹ Å ⁻¹)
Z3AA0104T	228.4428	0.111	4352	1222.5-1258.6	$4.364 \times 10^{-13} \pm 0.008^2$
Z3AA0106T	228.5083	0.159	4704	1532.3-1567.5	$2.673 \times 10^{-13} \pm 0.004^3$
Z3AA0108T	228.5798	0.209	4484	1225.5-1258.6	$4.564 \times 10^{-13} \pm 0.008^2$
Z3AA010AT	228.6511	0.259	4424	1532.3-1567.5	$2.761 \times 10^{-13} \pm 0.004^3$
Z3AA010CT	228.7223	0.312	4423	1225.5-1258.6	$4.457 \times 10^{-13} \pm 0.008^2$
Z3AA010ET	228.7926	0.360	4543	1532.3-1567.5	$2.600 \times 10^{-13} \pm 0.004^3$
Z3AA010GT	228.8619	0.410	4721	1225.5-1258.6	$4.177 \times 10^{-13} \pm 0.007^2$
Z3AA010IT	228.9285	0.465	6628	1532.3-1567.5	$2.411 \times 10^{-13} \pm 0.004^3$

¹Using the ephemeris of Woo *et al.* (1996) with the nth eclipse in JD given by $a_0 + a_1 * n + a_2 * n^2$ where $a_0 = \text{JD } 2,446,729.84878 \pm 0.0041$, $a_1 = 1.40840249 \pm 6.0 \times 10^{-7}$ days, and $a_2 = -1.45\text{E-}9$. $\phi_{orb}^0 = a_0$ and $P_{orb} = a_1 + a_2 * n$.

²Flux near N V ([1226-1234Å]+[1255-1259Å]).

³Flux near C IV ([1532-1544Å]+[1556-1567Å]).

4. FIGURES

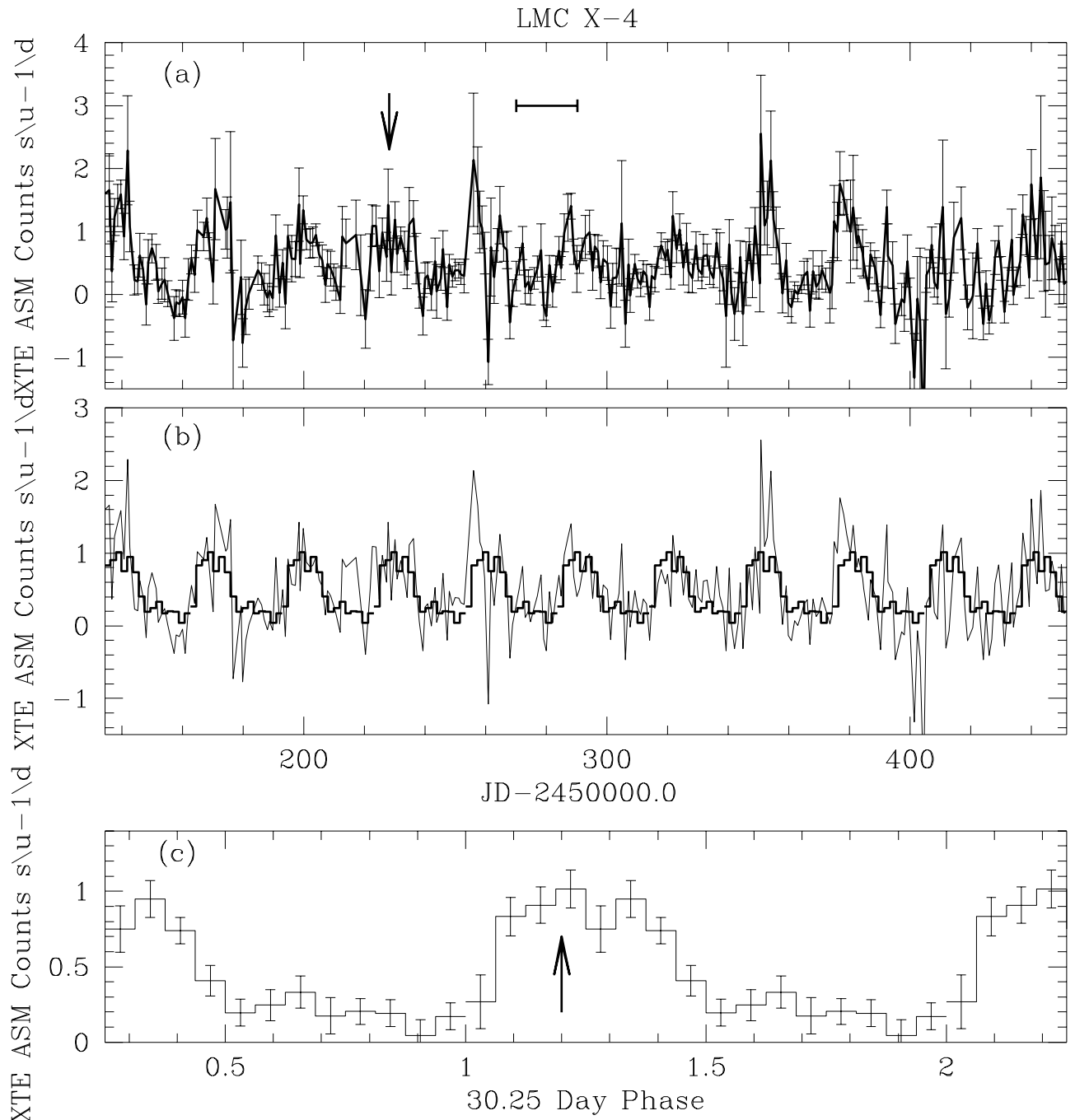


Figure 1.

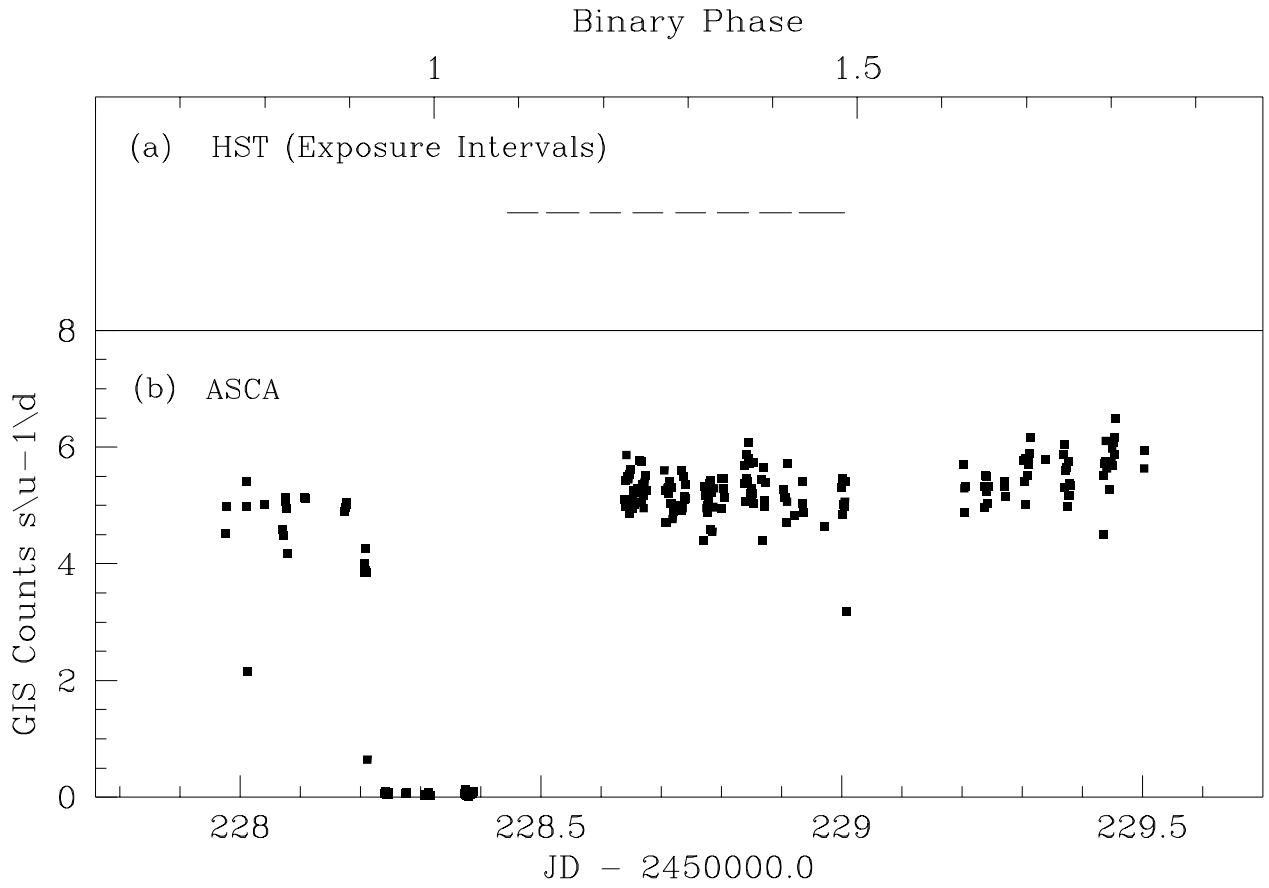


Figure 2.

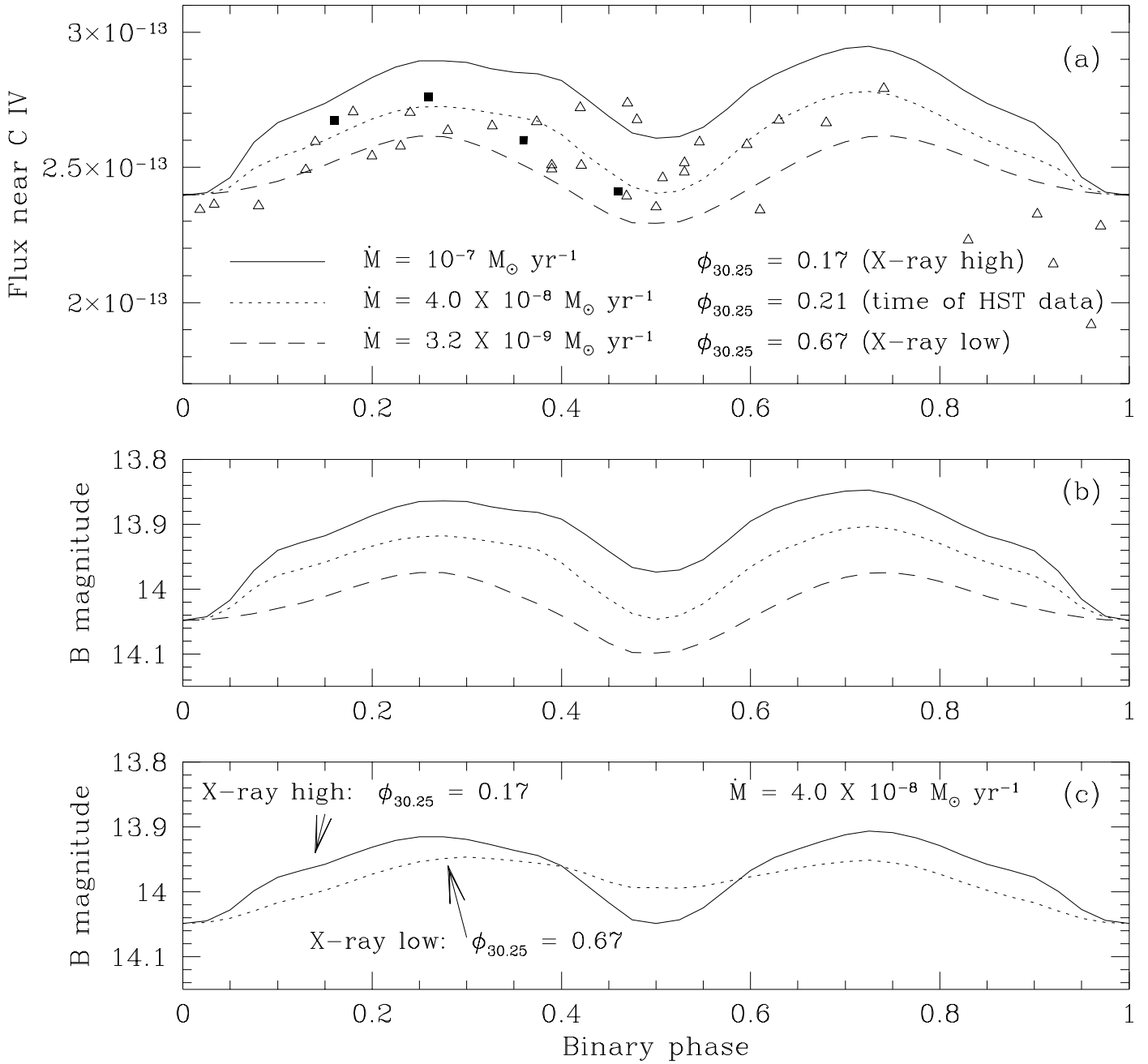


Figure 3.

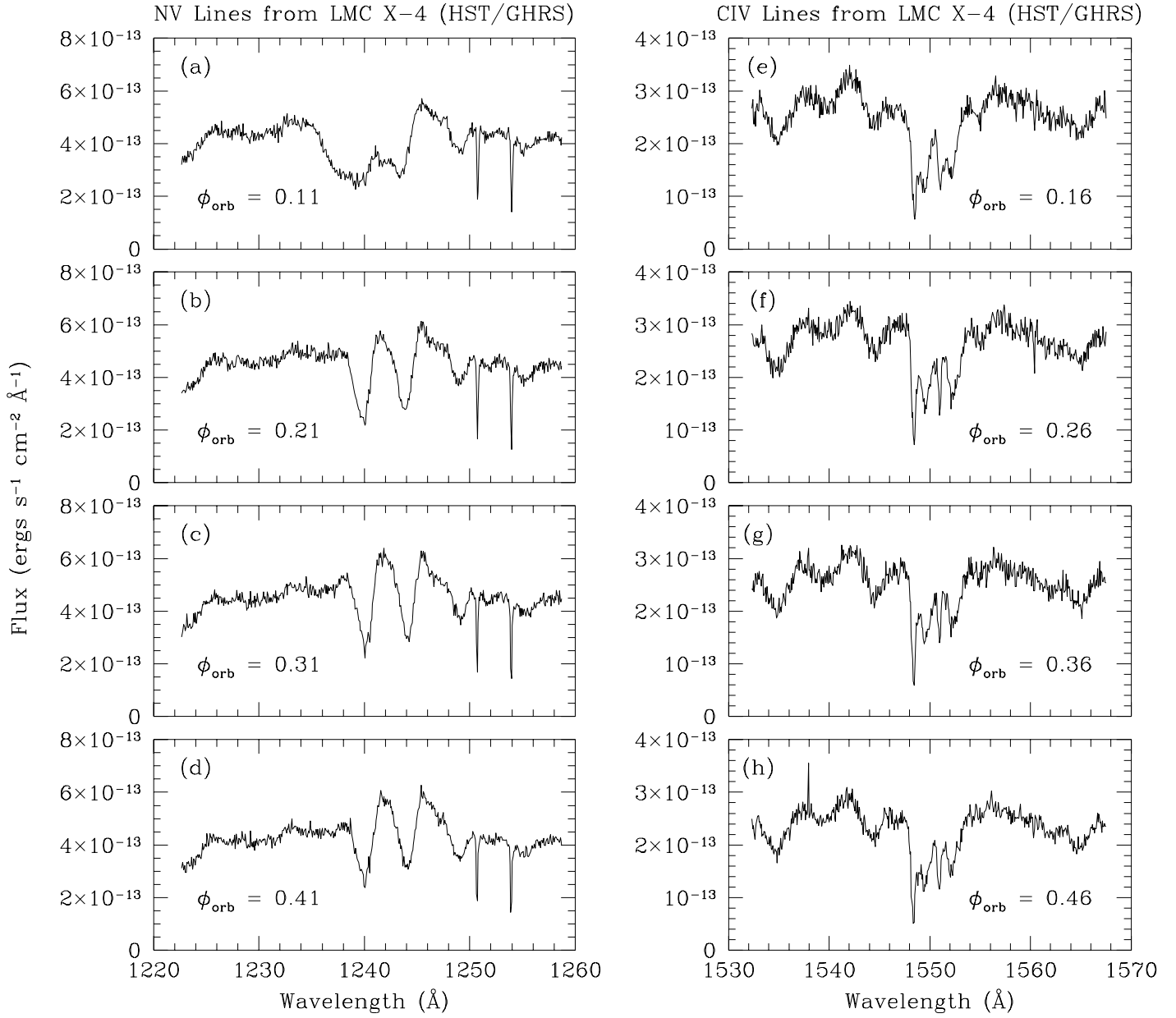


Figure 4.

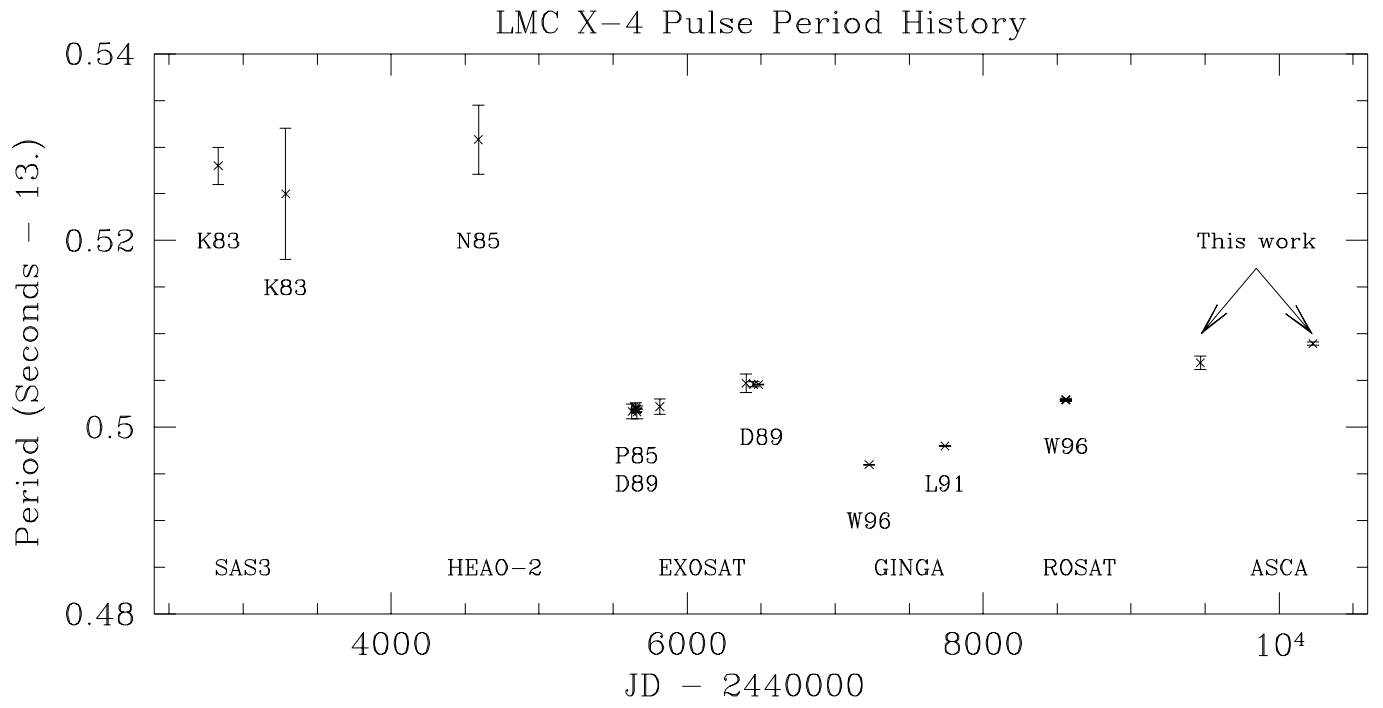


Figure 5.